Large Molecular Quadratic Hyperpolarizabilities in Donor/Acceptor-Substituted *trans*-Tetraammineruthenium(II) Complexes

Benjamin J. Coe,*,† Michelle C. Chamberlain,† Jonathan P. Essex-Lopresti,† Simon Gaines,† John C. Jeffery,‡ Stephan Houbrechts,§ and André Persoons§,||

Department of Chemistry, University of Manchester, Oxford Road, Manchester M13 9PL, U.K., Department of Chemistry, University of Bristol, Cantock's Close, Bristol BS8 1TS, U.K., Laboratory of Chemical and Biological Dynamics, Center for Research on Molecular Electronics and Photonics, University of Leuven, Celestijnenlaan 200D, B-3001 Leuven, Belgium, and Optical Sciences Center, University of Arizona, Tucson, Arizona, AZ 85721

Received December 6, 1996[⊗]

A series of new Ru(II) complex salts *trans*-$[Ru(NH_3)_4(L^1)(L^2)](PF_6)_n$ [$n = 2$, L^1 = 4-acetylpyridine (4-acpy) and L^2 = 4-(dimethylamino)pyridine (dmap) (**1**), 4-(dimethylamino)benzonitrile (dmabn) (**2**), 4-picoline (4-pic) (**3**), or 1-methylimidazole (1-MeIm) (**4**); $n = 3$, L^1 = *N*-methyl-4,4′-bipyridinium (MeQ^+) and L^2 = dmap (**6**), dmabn (**7**), 1-MeIm (**8**), 4-acpy (**9**), or phenothiazine (PTZ) (**10**); $n = 2$, L^1 = dmap and L^2 = 4-pyridinecarboxaldehyde (pyca) (**12**) or ethyl isonicotinate (isne) (**13**)] have been synthesized and fully characterized. These complexes display intense, visible metal-to-ligand charge-transfer (MLCT) absorptions which are highly solvatochromic. An X-ray crystal structure determination has been carried out for *trans*-$[Ru(NH_3)_4(MeQ^+)(PTZ)](PF_6)_3 \cdot Me_2CO$ (**10**·Me_2CO). This salt, empirical formula $C_{26}H_{38}F_{18}N_7OP_3RuS$, crystallizes in the hexagonal system, space group $P6_3$, with $a = b = 17.853(4)$ Å, $c = 21.514(6)$ Å, and $Z = 6$. The MeQ^+ ligand adopts an almost planar conformation, with a torsion angle of 9.6° between the two pyridyl rings. The dipolar cations exhibit a strong projected component along the *z* axis, but crystal twinning precludes second-harmonic generation. Measurements of the first hyperpolarizability β by using the hyper-Rayleigh scattering technique at 1064 nm yield very large values in the range $(232-621) \times 10^{-30}$ esu, the largest being for *trans*-$[Ru(NH_3)_4(MeQ^+)(dmabn)](PF_6)_3$ (**7**). These β values are resonance enhanced via the MLCT excitations. A correlation between β and the MLCT absorption energy confirms that this excitation is the primary contributor to β. The two-level model yields static hyperpolarizabilities β_0 in the range $(10-130) \times 10^{-30}$ esu, with *trans*-$[Ru(NH_3)_4(MeQ^+)(dmap)](PF_6)_3$ (**6**) having the largest. The β_0 values of the complexes of the bipyridyl ligand MeQ^+ are larger than those of their analogues containing monopyridyl ligands because of extended conjugation. β_0 correlates with the MLCT energy only when the MLCT absorption is sufficiently far from the second harmonic at 532 nm.

Introduction

There has recently been an explosion of interest in the study of organic compounds for potential applications in nonlinear optics (NLO).[1] This topic is at the forefront of current research because NLO materials will form the basis of the advanced electronics systems of the next century. As a part of this burgeoning field, organotransition metal complexes have received a limited degree of attention,[2] but their vast potential remains largely untapped. Metal complexes allow the combination of NLO with redox and magnetic properties, opening up possibilities unavailable with purely organic materials. Great scope exists within this area for developments based on novel synthetic coordination chemistry.

Most empirical studies on metal complexes for NLO have concentrated on bulk properties, the occurrence of quadratic effects being probed by powder second-harmonic generation (SHG).[3] This approach has some value as a crude screening technique but provides limited information due to complications arising from solid-state factors. An absence of SHG often results from the adoption of an unfavorable crystal packing by an otherwise NLO-active complex.[3b] For a fuller understanding of the molecular-level origins of NLO effects in metal complexes, it is necessary to measure hyperpolarizability tensors which can be correlated directly with molecular structure. This is generally more appropriate for the first hyperpolarizability β which governs quadratic nonlinearities. Recent examples for which the relationships between β and molecular structure have been investigated, albeit to a limited extent, include bimetallic sesquifulvalene complexes[4] and M(II) Schiff base complexes (M = Cu, Ni, Zn).[5]

A combination of attractive redox and spectroscopic properties with a vast coordination chemistry[6] renders ruthenium complexes ideal as NLO materials. Indeed, recent reports

* Corresponding author. E-mail: b.coe@man.ac.uk.
† University of Manchester.
‡ University of Bristol.
§ University of Leuven.
|| University of Arizona.
⊗ Abstract published in *Advance ACS Abstracts,* June 15, 1997.

(1) (a) *Nonlinear Optical Properties of Organic Molecules and Crystals*; Chemla, D. S., Zyss, J., Eds.; Academic Press: Orlando, FL, 1987; Vols. 1 and 2. (b) *Materials for Nonlinear Optics: Chemical Perspectives*; Marder, S. R., Sohn, J. S., Stucky, G. D., Eds.; ACS Symposium Series 455; American Chemical Society: Washington, DC, 1991. (c) Wagnière, G. H. *Linear and Nonlinear Optical Properties of Molecules*; VCH: Weinheim, Germany, 1993. (d) *Molecular Nonlinear Optics*; Zyss, J., Ed.; Academic Press: New York, 1994.

(2) (a) Marder, S. R. In *Inorganic Materials*; Bruce, D. W., O'Hare, D., Eds.; Wiley: Chichester, U.K., 1992. (b) Kanis, D. R.; Ratner, M. A.; Marks, T. J. *Chem. Rev.* **1994**, *94*, 195. (c) Long, N. J. *Angew. Chem., Int. Ed. Engl.* **1995**, *34*, 21.

(3) See, for example: (a) Coe, B. J.; Foulon, J.-D.; Hamor, T. A.; Jones, C. J.; McCleverty, J. A.; Bloor, D.; Cross, G. H.; Axon, T. L. *J. Chem. Soc., Dalton Trans.* **1994**, 3427. (b) Coe, B. J.; Hamor, T. A.; Jones, C. J.; McCleverty, J. A.; Bloor, D.; Cross, G. H.; Axon, T. L. *J. Chem. Soc., Dalton Trans.* **1995**, 673.

S0020-1669(96)01465-6 CCC: $14.00

indicate that ruthenium mixed-valence,[7] 2,2′-bipyridine (bpy),[8] and σ-acetylide[9] complexes can exhibit extremely large β values, although it appears that two-photon-excited luminescence, rather than harmonic scattering, may explain these results for the bpy complexes.[10] Other types of ruthenium complexes, the NLO properties of which have yet to be studied, hold great promise as high β molecules in which structure−property relationships may be elucidated.

Spectroscopic[11,12] and structural[13] studies on the complexes *trans*-$[Ru(NH_3)_4(L)(L')]^{n+}$ (L, L′ = unsaturated N-heterocycles; $n = 2, 3$) show that coplanarity of the axial ligands allows $\pi-\pi$ coupling through the polarizable Ru center. When combined with appropriate ligand substituents to create a dipole, this is expected to lead to large β values. These complexes are structurally versatile owing to a synthetic strategy based on *trans*-$[Ru^{II}Cl(NH_3)_4(SO_2)]Cl$,[14,15] which allows for various *trans* ligand combinations. The objectives of this work are the synthesis of a series of complexes *trans*-$[Ru^{II}(NH_3)_4(L^A)(L^D)]^{n+}$ (L^A, L^D = acceptor/donor-substituted ligands; $n = 2, 3$) and the assessment of their quadratic NLO properties via β measurements using the recently developed hyper-Rayleigh scattering (HRS) technique.[16,17] The HRS method has the important advantage over the more traditional electric-field-induced second-harmonic-generation (EFISHG) technique in that it is applicable to charged compounds, such as complex salts. An additional attractive feature of ruthenium ammine complexes is that the readily accessible $Ru^{III/II}$ redox couple provides a potential means for reversible, molecular-level modulation of NLO properties.

Experimental Section

Materials and Procedures. $RuCl_3 \cdot 2H_2O$ was supplied by Johnson Matthey plc. The salts *trans*-$[Ru^{II}Cl(NH_3)_4(SO_2)]Cl$ and *trans*-$[Ru^{III}(SO_4)(NH_3)_4(4\text{-acpy})]Cl$ were prepared according to published procedures.[18,19] The synthesis of $[MeQ^+]I$ described herein gives a greatly improved yield compared to that of a previous report.[18] All other reagents were obtained commercially and used as supplied. Products were dried overnight at room temperature in a vacuum desiccator ($CaSO_4$) prior to characterization.

Physical Measurements. ^1H NMR spectra were recorded on a Varian Gemini 200 spectrometer, and all shifts are referenced to TMS. The fine splitting of pyridyl or phenyl ring AA′BB′ patterns is ignored, and the signals are reported as simple doublets. Elemental analyses were performed by the Microanalytical Laboratory, University of Manchester. IR spectra were obtained as KBr disks with an ATI Mattson Genesis Series FTIR instrument. UV−visible spectra were recorded with a Hewlett-Packard 8452A diode array spectrophotometer. FAB mass spectra were recorded on a Kratos Concept spectrometer with a 6−8 keV Xe atom beam and 3-nitrobenzyl alcohol as matrix.

Cyclic voltammetric measurements were carried out using an EG&G PAR Model 173 potentiostat with an EG&G PAR Model 175 universal programmer. A single compartment cell was used with the SCE reference electrode separated by a salt bridge from the Pt bead working electrode and Pt wire auxiliary electrode. HPLC grade acetonitrile was used as received, and $[N(n\text{-}C_4H_9)_4]PF_6$, twice recrystallized from ethanol and dried in vacuo, was used as supporting electrolyte. Solutions containing *ca.* 10^{-3} M analyte (0.1 M electrolyte) were deaerated by N_2 purging. All $E_{1/2}$ values were calculated from $(E_{pa} + E_{pc})/2$ at a scan rate of 200 mV s^{-1}.

Synthesis of *N*-Methyl-4,4′-bipyridinium Iodide, $[MeQ^+]I$. A solution of 4,4′-bipyridine (3.01 g, 19.3 mmol) and methyl iodide (5 mL, 80.3 mmol) in chloroform (100 mL) was stirred at room temperature for 3 d. The yellow precipitate was collected by filtration, washed with chloroform, and dried. Purification was effected by recrystallization from ethanol to afford a golden solid (3.68 g). A further 940 mg of product (after recrystallization) was obtained from the reaction filtrate solution after standing for 7 d, to give a total yield of 4.62 g, 80%; δ_H (D_2O) 8.85 (2 H, d, $J = 7.2$ Hz, C_5H_4N−Me), 8.67 (2 H, d, $J = 6.4$ Hz, C_5H_4N), 8.31 (2 H, d, $J = 6.9$ Hz, C_5H_4N−Me), 7.82 (2 H, d, $J = 6.3$ Hz, C_5H_4N), 4.39 (3 H, s, Me). Anal. Calcd for $C_{11}H_{11}IN_2$: C, 44.32; H, 3.72; N, 9.40; I, 42.57. Found: C, 44.67; H, 3.57; N, 9.27; I, 42.30.

Synthesis of *trans*-$[Ru^{II}(NH_3)_4(4\text{-acpy})(dmap)](PF_6)_2$ (1). A solution of *trans*-$[Ru^{III}(SO_4)(NH_3)_4(4\text{-acpy})]Cl$ (120 mg, 0.284 mmol) in water (10 mL) was reduced over zinc amalgam (five lumps) with Ar agitation for 15 min. The resulting solution was filtered under Ar into a flask containing 4-(dimethylamino)pyridine (dmap; 200 mg, 1.64 mmol), and the filtrate was stirred at room temperature in the dark under Ar for 3 h. The addition of aqueous NH_4PF_6 to the deep purple solution gave a dark precipitate, which was collected by filtration, washed with water, and dried. The product was precipitated from acetone/aqueous NH_4PF_6 and then from acetone/diethyl ether to afford a dark red-purple solid: yield 98 mg, 49%; δ_H (CD_3COCD_3) 9.02 (2 H, d, $J = 6.8$ Hz, Ac−*py*), 8.29 (2 H, d, $J = 7.2$ Hz, Me_2N−*py*), 7.76 (2 H, d, $J = 6.8$ Hz, Ac−*py*), 6.85 (2 H, d, $J = 7.2$ Hz, Me_2N−*py*), 3.15 (6 H, s, Me_2N−py), 2.71 (12 H, br s, 4 × NH_3), 2.62 (3 H, s, *Ac*−py); ν(C═O) 1692 (m) cm^{-1}. Anal. Calcd for $C_{14}H_{29}F_{12}N_7OP_2Ru$: C, 23.94; H, 4.16; N, 13.96. $[M - PF_6^-] = 557$. Found: C, 24.14; H, 4.39; N, 13.66. $[M - PF_6^-]^+ = 558$.

Synthesis of *trans*-$[Ru^{II}(NH_3)_4(4\text{-acpy})(dmabn)](PF_6)_2$ (2). This was prepared and purified identically to **1** by using 4-(dimethylamino)-benzonitrile (dmabn; 240 mg, 1.64 mmol) in acetone (5 mL) in place of dmap. The product was obtained as an orange solid: yield 139 mg, 67%; δ_H (CD_3COCD_3) 9.09 (2 H, d, $J = 6.8$ Hz, Ac-*py*), 7.84 (2 H, d, $J = 6.8$ Hz, Ac−*py*), 7.67 (2 H, d, $J = 9.2$ Hz, Me_2N−C_6H_4−CN), 6.85 (2 H, d, $J = 9.2$ Hz, Me_2N−C_6H_4−CN), 3.10 (6 H, s, Me_2N−C_6H_4−CN), 2.77 (12 H, br s, 4 × NH_3), 2.65 (3 H, s, *Ac*−py); ν(C≡N) 2211 (vw), ν(C═O) 1697 (m) cm^{-1}. Anal. Calcd for $C_{16}H_{29}F_{12}N_7OP_2Ru$: C, 26.45; H, 4.02; N, 13.50. $[M - PF_6^-] = 581$. Found: C, 26.54; H, 3.91; N, 13.90. $[M - PF_6^-]^+ = 582$.

Synthesis of *trans*-$[Ru^{II}(NH_3)_4(4\text{-acpy})(4\text{-pic})](PF_6)_2$ (3). This was prepared and purified identically to **1** by using 4-picoline (4-pic; 0.15 mL, 1.55 mmol) in place of dmap. The product was obtained as a red-brown solid: yield 36 mg, 19%; δ_H (CD_3COCD_3) 9.06 (2 H, d, $J = 6.6$ Hz, Ac-*py*), 8.69 (2 H, d, $J = 6.2$ Hz, Me−*py*), 7.82 (2 H, d, $J = 6.8$ Hz, Ac−*py*), 7.43 (2 H, d, $J = 5.9$ Hz, Me−*py*), 2.76 (12 H, br s, 4 × NH_3), 2.65 (3 H, s, *Ac*−py), 2.49 (3 H, s, *Me*−py); ν(C═O) 1696 (m) cm^{-1}. Anal. Calcd for $C_{13}H_{26}F_{12}N_6OP_2Ru$: C, 23.19; H,

(4) Behrens, U.; Brussaard, H.; Hagenau, U.; Heck, J.; Hendrickx, E.; Körnich, J.; van der Linden, J. G. M.; Persoons, A.; Spek, A. L.; Veldman, N.; Voss, B.; Wong, H. *Chem. Eur. J.* **1996**, *2*, 98.
(5) (a) Di Bella, S.; Fragala, I.; Ledoux, I.; Marks, T. J. *J. Am. Chem. Soc.* **1995**, *117*, 9481. (b) Lacroix, P. G.; Di Bella, S.; Ledoux, I. *Chem. Mater.* **1996**, *8*, 541.
(6) Schröder, M.; Stephenson, T. A. In *Comprehensive Coordination Chemistry*; Wilkinson, G., Gillard, R. D., McCleverty, J. A., Eds.; Pergamon Press: Oxford, U.K., 1987; Vol. 4.
(7) (a) Laidlaw, W. M.; Denning, R. G.; Verbiest, T.; Chauchard, E.; Persoons, A. *Nature* **1993**, *363*, 58. (b) Laidlaw, W. M.; Denning, R. G.; Verbiest, T.; Chauchard, E.; Persoons, A. *Proc. SPIE-Int. Soc. Opt. Eng.* **1994**, *2143*, 14.
(8) (a) Zyss, J.; Dhenaut, C.; Chauvan, T.; Ledoux, I. *Chem. Phys. Lett.* **1993**, *206*, 409. (b) Dhenaut, C.; Ledoux, I.; Samuel, I. D. W.; Zyss, J.; Bourgault, M.; Le Bozec, H. *Nature* **1995**, *374*, 339.
(9) Whittall, I. R.; Humphrey, M. G.; Persoons, A.; Houbrechts, S. *Organometallics* **1996**, *15*, 1935.
(10) Morrison, I. D.; Denning, R. G.; Laidlaw, W. M.; Stammers, M. A. *Rev. Sci. Instrum.* **1996**, *67*, 1445.
(11) Zwickel, A. M.; Creutz, C. *Inorg. Chem.* **1971**, *10*, 2395.
(12) Tfouni, E.; Ford, P. C. *Inorg. Chem.* **1980**, *19*, 72.
(13) (a) Wishart, J. F.; Zhang, X.; Isied, S. S.; Potenza, J. A.; Schugar, H. J. *Inorg. Chem.* **1992**, *31*, 3179. (b) LaChance-Galang, K. J.; Doan, P. E.; Clarke, M. J.; Rao, U.; Yamano, A.; Hoffman, B. M. *J. Am. Chem. Soc.* **1995**, *117*, 3529.
(14) Isied, S. S.; Taube, H. *Inorg. Chem.* **1976**, *15*, 3070.
(15) Marchant, J. A.; Matsubara, T.; Ford, P. C. *Inorg. Chem.* **1977**, *16*, 2160.
(16) (a) Clays, K.; Persoons, A. *Phys. Rev. Lett.* **1991**, *66*, 2980. (b) Clays, K.; Persoons, A. *Rev. Sci. Instrum.* **1992**, *63*, 3285.
(17) Hendrickx, E.; Clays, K.; Persoons, A.; Dehu, C.; Brédas, J. L. *J. Am. Chem. Soc.* **1995**, *117*, 3547.
(18) Curtis, J. C.; Sullivan, B. P.; Meyer, T. J. *Inorg. Chem.* **1983**, *22*, 224.
(19) Chang, J. P.; Fung, E. Y.; Curtis, J. C. *Inorg. Chem.* **1986**, *25*, 4233.

3.89; N, 12.48. [M − PF_6^-] = 528. Found: C, 23.18; H, 3.81; N, 12.25. [M − PF_6^-]$^+$ = 529.

Synthesis of *trans*-[$Ru^{II}(NH_3)_4$(4-acpy)(1-MeIm)]$(PF_6)_2$ (4). This was prepared and purified identically to **1** by using 1-methylimidazole (1-MeIm; 0.15 mL, 1.87 mmol) in place of dmap. The product was obtained as a deep burgundy-colored solid: yield 96 mg, 51%; δ_H (CD_3COCD_3) 9.06 (2 H, d, J = 6.8 Hz, Ac-*py*), 8.17 (1 H, s, Im), 7.72 (2 H, d, J = 6.8 Hz, Ac-*py*), 7.44 (1 H, t, J = 1.4 Hz, Im), 7.36 (1 H, t, J = 1.4 Hz, Im), 3.90 (3 H, s, *Me*-Im), 2.64 (12 H, br s, 4 × NH_3), 2.62 (3 H, s, *Ac*-py); ν(C═O) 1689 cm^{-1}. Anal. Calcd for $C_{11}H_{25}F_{12}N_7OP_2Ru$: C, 19.95; H, 3.80; N, 14.80. [M − PF_6^-] = 517. Found: C, 19.75; H, 4.10; N, 14.53. [M − PF_6^-]$^+$ = 518.

Synthesis of *trans*-[$Ru^{III}(SO_4)(NH_3)_4(MeQ^+)$]$Cl_2$ (5). A mixture of *trans*-[$Ru^{II}Cl(NH_3)_4(SO_2)$]Cl (100 mg, 0.329 mmol) and [MeQ^+]I (490 mg, 1.64 mmol) was dissolved in water (5 mL), and the solution was heated at *ca*. 45 °C under Ar for 30 min. The dark brown solution and solid were added to acetone (100 mL), and the mixture was allowed to settle in a refrigerator for 30 min. The brown solid was collected by filtration, washed with acetone, and dried. This material (a mixture of the chloride or iodide salts of *trans*-[$Ru^{II}(NH_3)_4(SO_2)(MeQ^+)]^{3+}$ and unreacted [MeQ^+]I) was then dissolved in water (*ca*. 10 mL) and oxidized by addition of a 1/1 mixture of 30% aqueous H_2O_2 solution/2 M HCl (3 mL). After 5 min at room temperature, the brown precipitate was removed by filtration, washed with water, and discarded. Acetone (150 mL) was added to the yellow filtrate, and the mixture was then stored at 4 °C overnight to yield the product as a yellow oil. The pale yellow solution was decanted off, and the oil was washed with acetone and dried to afford a sticky solid. This material was unweighed and the same quantity was used in the subsequent syntheses of **6**−**10** without further purification. The yields for **6**−**10** are hence quoted with respect to *trans*-[$Ru^{II}Cl(NH_3)_4(SO_2)$]Cl.

Synthesis of *trans*-[$Ru^{II}(NH_3)_4(MeQ^+)$(dmap)]$(PF_6)_3$ (6). This was prepared and purified identically to **1** by using **5** in place of *trans*-[$Ru^{III}(SO_4)(NH_3)$(4-acpy)]Cl. The product was obtained as an indigo solid: 116 mg, 39%; δ_H (CD_3COCD_3) 9.10 (4 H, m, C_5H_4N−Me and C_5H_4N), 8.69 (2 H, d, J = 7.0 Hz, C_5H_4N−Me), 8.31 (2 H, d, J = 7.2 Hz, NC_5H_4−NMe_2), 7.99 (2 H, d, J = 7.0 Hz, C_5H_4N), 6.87 (2 H, d, J = 7.2 Hz, NC_5H_4-NMe_2), 4.58 (3 H, s, Me), 3.16 (6 H, s, NMe_2), 2.75 (12 H, s, 4 × NH_3). Anal. Calcd for $C_{18}H_{33}F_{18}N_8P_3Ru$: C, 24.09; H, 3.71; N, 12.49. [M − PF_6^-] = 753; [M − 2(PF_6^-)] = 608; [M − 3(PF_6^-)] = 463. Found: C, 24.13; H, 3.88, N, 11.85. [M − PF_6^-]$^+$ = 753; [M − 2(PF_6^-)]$^+$ = 608; [M − 3(PF_6^-)]$^+$ = 464.

Synthesis of *trans*-[$Ru^{II}(NH_3)_4(MeQ^+)$(dmabn)]$(PF_6)_3$ (7). This was prepared and purified identically to **2** by using **5** in place of *trans*-[$Ru^{III}(SO_4)(NH_3)_4$(4-acpy)]Cl. The product was obtained as a red-brown solid: 141 mg, 47%; δ_H (CD_3COCD_3) 9.18−9.13 (4 H, m, C_5H_4N−Me and C_5H_4N), 8.70 (2 H, d, J = 7.0 Hz, C_5H_4N−Me), 8.07 (2 H, d, J = 7.0 Hz, C_5H_4N), 7.68 (2 H, d, J = 9.2 Hz, Me_2N−C_6H_4−CN), 6.86 (2 H, d, J = 9.2 Hz, Me_2N−C_6H_4−CN), 4.62 (3 H, s, Me), 3.10 (6 H, s, NMe_2), 2.81 (12 H, s, 4 × NH_3). Anal. Calcd for $C_{20}H_{33}F_{18}N_8P_3Ru$: C, 26.07; H, 3.61; N, 12.16. [M − PF_6^-] = 777; [M − 2(PF_6^-)] = 632; [M − 3(PF_6^-)] = 487. Found: C, 26.63; H, 3.38; N, 11.85. [M − PF_6^-]$^+$ = 777; [M − 2(PF_6^-)]$^+$ = 632; [M − 3(PF_6^-)]$^+$ = 488.

Synthesis of *trans*-[$Ru^{II}(NH_3)_4(MeQ^+)$(1-MeIm)]$(PF_6)_3$ (8). This was prepared and purified identically to **3** by using **5** in place of *trans*-[$Ru^{III}(SO_4)(NH_3)_4$(4-acpy)]Cl. The product was obtained as an indigo solid: 156 mg, 55%; δ_H (CD_3COCD_3) 9.15 (2 H, d, J = 7.0 Hz, C_5H_4N−Me), 9.09 (2 H, d, J = 7.0 Hz, C_5H_4N), 8.69 (2 H, d, J = 7.0 Hz, C_5H_4N−Me), 8.21 (1 H, s, Im), 7.95 (2 H, d, J = 7.0 Hz, C_5H_4N), 7.46 (1 H, s, Im), 7.38 (1 H, t, J = 1.5 Hz, Im), 4.57 (3 H, s, C_5H_4N−*Me*), 3.92 (3 H, s, *Me*−Im), 2.69 (12 H, s, 4 × NH_3). Anal. Calcd for $C_{15}H_{29}F_{18}N_8P_3Ru$: C, 21.01; H, 3.41; N, 13.07. [M − PF_6^-] = 712; [M − 2(PF_6^-)] = 567; [M − 3(PF_6^-)] = 422. Found: C, 21.16; H, 3.36; N, 12.96. [M − PF_6^-]$^+$ = 713; [M − 2(PF_6^-)$^+$ = 568; [M − 3(PF_6^-)]$^+$ = 424.

Synthesis of *trans*-[$Ru^{II}(NH_3)_4(MeQ^+)$(4-acpy)]$(PF_6)_3$ (9). This was prepared and purified identically to **6** by using 4-acetylpyridine (4-acpy; 0.2 mL, 1.81 mmol) in place of dmap. The product was obtained as a dark red solid: 55 mg, 19%; δ_H (CD_3COCD_3) 9.19−9.11 (6 H, m, C_5H_4N−Me, C_5H_4N, and Ac−*py*), 8.71 (2 H, d, J = 7.0 Hz, C_5H_4N−Me), 8.13 (2 H, d, J = 6.9 Hz, C_5H_4N), 7.92 (2 H, d, J = 6.8 Hz, Ac-*py*), 4.63 (3 H, s, C_5H_4N−*Me*), 2.85 (12 H, s, 4 × NH_3), 2.68 (3 H, s, *Ac*−py); ν(C═O) 1692 (m) cm^{-1}. Anal. Calcd for $C_{18}H_{30}F_{18}N_7P_3Ru$: C, 24.56; H, 3.43; N, 11.14. [M − 3(PF_6^-)] = 445. Found: C, 24.28; H, 3.50; N, 10.94. [M − 3(PF_6^-)]$^+$ = 443.

Synthesis of *trans*-[$Ru^{II}(NH_3)_4(MeQ^+)$(PTZ)]$(PF_6)_3$ (10). A solution of **5** in water (10 mL) was reduced over zinc amalgam (5 lumps) with Ar agitation for 15 min, and the resulting solution was filtered under Ar into a flask containing acetone (150 mL). After refrigeration, the deep blue precipitate was collected by filtration, washed with acetone, and dried to yield a turquoise solid (150 mg). This was dissolved in water (5 mL), and the solution was added to solid NH_4PF_6 (1.0 g). After refrigeration, the deep purple precipitate was collected by filtration and dried and then dissolved in acetone (10 mL), and phenothiazine (PTZ; 434 mg, 2.18 mmol) was added. The deep blue solution turned purple within minutes and was stirred in the dark under Ar for 1 h to yield a deep burgundy-colored solution. The addition of diethyl ether afforded a dark precipitate, which was collected by filtration, washed with diethyl ether, and dried. Purification was effected by precipitation from acetone/aqueous NH_4PF_6 to yield a dark red solid: 221 mg, 69%; δ_H (CD_3COCD_3) 9.14 (2 H, d, J = 6.8 Hz, C_5H_4N−Me), 8.89 (2 H, d, J = 6.9 Hz, C_5H_4N), 8.71 (1 H, s, NH), 8.63 (2 H, d, J = 7.0 Hz, C_5H_4N−Me), 8.12 (2 H, d, J = 6.9 Hz, C_5H_4N), 7.56 (2 H, d, J = 7.8 Hz, PTZ), 7.44−7.36 (2 H, m, PTZ), 7.20−7.12 (4 H, m, PTZ), 4.62 (3 H, s, C_5H_4N−*Me*), 2.59 (12 H, s, 4 × NH_3). Anal. Calcd for $C_{23}H_{32}F_{18}N_7P_3RuS{\cdot}C_3H_6O$: C, 30.24; H, 3.71; N, 9.49; S, 3.11. [M − PF_6^-] = 830; [M − 2(PF_6^-)] = 685; [M − 3(PF_6^-)] = 540. Found: C, 29.90; H, 3.51; N, 9.42; S, 2.94. [M − PF_6^-]$^+$ = 830; [M − 2(PF_6^-)]$^+$ = 687; [M − 3(PF_6^-)]$^+$ = 542.

Synthesis of trans-[$Ru^{III}(SO_4)(NH_3)_4$(dmap-*N*-O)]Cl (11). A mixture of *trans*-[$Ru^{II}Cl(NH_3)_4(SO_2)$]Cl (100 mg, 0.329 mmol) and dmap (2.01 g, 16.5 mmol) was dissolved in water (3 mL), and the solution was heated at *ca*. 45 °C under Ar for 30 min. The pale green solution was added to acetone (100 mL), and the mixture was allowed to settle in a refrigerator. The pale mauve solid was collected by filtration, washed with acetone, and dried (135 mg). This material was then dissolved in water (*ca*. 5 mL) and oxidized by addition of a 1/1 mixture of 30% aqueous H_2O_2 solution/2 M HCl (3 mL). After 5 min at room temperature, the purple solution was added to acetone (150 mL), and the mixture was allowed to settle in a refrigerator. The dark red precipitate was collected by filtration, washed with acetone, and dried (125 mg). This crude product was used in the same quantity for the syntheses of **12** and **13**, the yields of which are hence quoted with respect to *trans*-[$Ru^{II}Cl(NH_3)_4(SO_2)$]Cl.

Synthesis of *trans*-[$Ru^{II}(NH_3)_4$(dmap)(pyca)]$(PF_6)_2$ (12). This was prepared and purified similarly to **1** by using **11** in place of *trans*-[$Ru^{III}(SO_4)(NH_3)_4$(4-acpy)]Cl and using 4-pyridinecarboxaldehyde (pyca; 0.1 mL, 1.05 mmol) in place of dmap. During the reduction, the color of the aqueous solution of **11** changed from deep purple to golden-brown. A dark red-purple solid was obtained: 57 mg, 25%; δ_H (CD_3COCD_3) 10.18 (1 H, s, CHO), 9.09 (2 H, d, J = 6.5 Hz, *py*−CHO), 8.31 (2 H, d, J = 7.2 Hz, Me_2N−*py*), 7.72 (2 H, d, J = 6.7 Hz, *py*−CHO), 6.84 (2 H, d, J = 7.0 Hz, Me_2N−*py*), 3.21 (6 H, s, Me_2N−py), 2.79 (12 H, br s, 4 × NH_3); ν(C═O) 1706 (m) cm^{-1}. Anal. Calcd for $C_{13}H_{27}F_{12}N_7OP_2Ru$: C, 22.68; H, 3.95; N, 14.24. [M − PF_6^-] = 543; [M − 2(PF_6^-)] = 398. Found: C, 23.08; H, 3.78; N, 13.85. [M − PF_6^-]$^+$ = 544; [M − 2(PF_6^-)]$^+$ = 400.

Synthesis of *trans*-[$Ru^{II}(NH_3)_4$(dmap)(isne)]$(PF_6)_2$ (13). This was prepared and purified similarly to **12** by using ethyl isonicotinate (0.15 mL, 1.00 mmol) in place of pyca. After precipitation from acetone/diethyl ether, the product was precipitated twice more from acetone/aqueous NH_4PF_6 to afford an orange solid: 59 mg, 24%; δ_H (CD_3COCD_3) 9.00 (2 H, d, J = 6.7 Hz, *py*−CO_2Et), 8.28 (2 H, d, J = 7.2 Hz, Me_2N−*py*), 7.76 (2 H, d, J = 6.7 Hz, *py*−CO_2Et), 6.84 (2 H, d, J = 7.0 Hz, Me_2N−*py*), 4.41 (2 H, q, J = 7.1 Hz, pyCO_2−CH_2−Me), 3.15 (6 H, s, Me_2N−py), 2.70 (12 H, br s, 4 × NH_3), 1.38 (3 H, t, J = 7.1 Hz, pyCO_2CH_2−*Me*); ν(C═O) 1727 (s) cm^{-1}. Anal. Calcd for $C_{15}H_{31}F_{12}N_7O_2P_2Ru$: C, 24.60; H, 4.27; N, 13.39. [M − PF_6^-] = 587; [M − 2(PF_6^-)] = 442. Found: C, 24.74; H, 4.17; N, 12.90. [M − PF_6^-]$^+$ = 588; [M − 2(PF_6^-)]$^+$ = 444.

X-ray Structural Determination. Crystals of *trans*-[$Ru(NH_3)_4$(MeQ^+)(PTZ)]$(PF_6)_3{\cdot}Me_2CO$ (**10**·Me_2CO) were grown by diffusion of diethyl ether into an acetone solution containing added PTZ at 4 °C.

Crystallization in the absence of free PTZ produces a blue material due to slow loss of the PTZ ligand, a process which occurs even in the dark.

A red, hexagonal prismatic crystal of **10**·Me_2CO of dimensions 0.50 × 0.50 × 0.45 mm was mounted on a glass fiber, and data were collected on a Siemens SMART CCD area-detector three-circle diffractometer at low temperature. For three settings of ϕ, narrow data "frames" were collected for 0.3° increments in ω. A total of 1271 frames were collected, affording rather more than a hemisphere of data. At the end of data collection, the first 50 frames were recollected to establish that crystal decay had not taken place. The substantial redundancy in data allows empirical absorption corrections to be applied using multiple measurements of equivalent reflections. Data frames were collected for 10 s per frame, giving an overall data collection time of *ca*. 7 h. The data frames were integrated using SAINT.[20] The structure was solved by direct methods and refined by full-matrix least-squares calculations on all F_o^2 data using Siemens SHELXTL 5.03.[20] All non-hydrogen atoms were refined anisotropically. The NH hydrogen of the PTZ ligand was located and refined. All other hydrogen atoms were included in calculated positions with isotropic thermal parameters *ca*. 1.2 × (aromatic CH) or 1.5 × (Me) the equivalent isotropic thermal parameters of their parent carbon atoms. All calculations were carried out on Silicon Graphics Indy or Indigo computers. The asymmetric unit contains one molecule of the cation, two PF_6^- anions, and one molecule of acetone in general positions. In addition, there are three PF_2 fragments lying astride 3-fold axes. There are therefore a total of three PF_6^- anions per complex cation. The crystals are twinned (*ca*. 50:50, twin matrix 010, 100, 00$\bar{1}$).

ORTEP[21] diagrams showing two alternative views of the complex cation are given in Figure 3, and a packing diagram is shown in Figure 4. Crystallographic data and refinement details are presented in Table 3, and selected bond distances and angles, in Table 4. Additional material available from the Cambridge Crystallographic Data Centre comprises final atomic fractional coordinates, thermal parameters, and nonessential bond lengths and angles.

Hyper-Rayleigh Scattering. Details of the HRS experiment have been discussed previously,[16,17] and the experimental setup used was as described in a recent report.[22] First hyperpolarizabilities were obtained by using the external reference method (ERM),[22] with the EFISHG-derived β_{1064} value for 4-nitroaniline in acetonitrile of 29.2×10^{-30} esu.[23] The ERM has been found by the authors and by other workers[24,25] to give more reliable β values than the originally used internal reference method. All measurements were performed using the 1064 nm fundamental wavelength of an injection-seeded, Q-switched Nd:YAG laser (Quanta-Ray GCR-5, 8 ns pulses, 7 mJ, 10 Hz). Acetonitrile solutions were $10^{-4}-10^{-5}$ mol dm^{-3} in complex salt, the low concentrations being necessary to minimize absorptive losses. One-dimensional hyperpolarizability is assumed, *i.e.* $\beta_{1064} = \beta_{333}$, and a relative error of ±15% is estimated.

Results and Discussion

Synthetic Studies. The new complex salts were prepared by using established coordination chemistry based on *trans*-$[RuCl(NH_3)_4(SO_2)]Cl$.[12,14,15,18,19] For the synthesis of *trans*-$[Ru(NH_3)_4(MeQ^+)(PTZ)](PF_6)_3$ (**10**), the procedure was modified because of the insolubility of PTZ in water. Following zinc amalgam reduction of **5**, the intermediate *trans*-$[Ru(NH_3)_4(MeQ^+)(H_2O)]Cl_3$ was isolated by precipitation with acetone, metathesized to its PF_6^- salt, and reacted with PTZ in acetone to give **10** in good yield.

In the syntheses of *trans*-$[Ru(NH_3)_4(dmap)(L^A)](PF_6)_2$ [L^A = pyca (**12**), isne (**13**)], it was found that the use of a large excess (*ca*. 50-fold) of dmap in the first substitution reaction improves the yield and purity of the final products. By contrast, when 4-acpy or $[MeQ^+]I$ is used, a 5-fold excess is adequate. The precursor *trans*-$[RuCl(NH_3)_4(SO_2)]Cl$ clearly reacts less efficiently with the more basic dmap ligand in water, but the reasons for this are currently unclear. It is assumed that the $-NMe_2$ group in *trans*-$[Ru(NH_3)_4(dmap)(SO_2)]Cl_2$ is oxidized to the *N*-oxide by the acidic H_2O_2 solution[26] but subsequently re-reduced by the zinc amalgam. The presence of the intact $-NMe_2$ moiety in **12** and **13** is confirmed by ^1H NMR spectra. This hypothesis has not been proven by analysis of the intermediate **11**, but is supported by the observation that the color change upon reduction, which normally occurs rapidly, requires a longer time to reach completion with **11**. This implies a rapid reduction of Ru(III) followed by a slower reduction of the *N*-oxide group. The yields of **12** and **13** are substantially lower than those for most of the other salts, and the final purities as assessed by ^1H NMR are a little lower (*ca*. 95%).

The choice of ligands for this study was determined largely by the structural requirements for large β and by availability but was also limited somewhat by the reagents used in the oxidation and reduction stages which affect certain organic functional groups. The structures of the new complexes, excepting **5** and **11**, are shown in Figure 1.

^1H NMR Studies. All of the new Ru(II) complex salts give well-defined ^1H NMR spectra, which permit unambiguous identification and assessment of purity. A singlet in the region 2.81−2.59 ppm for the four ammine ligands confirms the *trans* geometry, and signals for all of the aromatic ligands are observed in their expected positions.

UV−Visible Studies. Spectra for all of the new complex salts, except for the intermediates **5** and **11**, were recorded in acetonitrile, and results are presented in Table 1.

All show intense, broad $d\pi(Ru^{II}) \rightarrow \pi^*(L)$ metal-to-ligand charge-transfer (MLCT) bands in the region 320−615 nm, the energies of which are related to the electron donor ability of the Ru center and to the electron-acceptor ability of L.[27,28] With the exceptions of **4** and **8**−**10**, two discrete bands are observed, one at low energy between 470 and 615 nm and the other at high energy in the region 320−360 nm. Similar spectra have been reported for related *trans*-$\{Ru(NH_3)_4\}^{2+}$ complexes.[12,18] The low-energy (MLCT-1) bands correspond to $d\pi(Ru^{II}) \rightarrow \pi^*(L^A)$ excitations where L^A = 4-acpy, MeQ^+, pyca, or isne, the π^* acceptor orbitals of which are stabilized by their electron-withdrawing substituents. The high-energy (MLCT-2) absorptions are due to $d\pi(Ru^{II}) \rightarrow \pi^*(L^D)$ excitations where L^D = dmap, dmabn, or 4-pic, the π^* acceptor orbitals of which are destabilized by their electron-donating substituents. In the case of **9**, overlapping visible MLCT bands are observed due to the presence of the two acceptor-substituted ligands, 4-acpy and MeQ^+. The separation of *ca*. 110 nm demonstrates the greater acceptor ability of the MeQ^+ ligand. For this salt, the $d\pi(Ru^{II}) \rightarrow \pi^*$(4-acpy) band is denoted MLCT-2 and 4-acpy is hence L^D.

In accord with previous reports,[12,18] the MLCT-2 energy is almost constant, whereas that of the MLCT-1 bands is markedly influenced by the nature of the *trans* ligand. For the salts *trans*-$[Ru(NH_3)_4(4\text{-acpy})(L^D)](PF_6)_2$ (**1**−**4**) the MLCT-1 energy in-

(20) *SHELXTL 5.03*; Siemens Analytical X-Ray Instruments: Madison, WI, 1995.
(21) Johnson, C. K. *ORTEP: A Fortran Thermal Ellipsoid Plot Program*; Technical Report ORNL-5138; Oak Ridge National Laboratory: Oak Ridge, TN, 1976.
(22) Houbrechts, S.; Clays, K.; Persoons, A.; Pikramenou, Z.; Lehn, J.-M. *Chem. Phys. Lett*. **1996**, *258*, 485.
(23) Stähelin, M.; Burland, D. M.; Rice, J. E. *Chem. Phys. Lett*. **1992**, *191*, 245.
(24) Stadler, S.; Bourhill, G.; Bräuchle, C. *J. Phys. Chem*. **1996**, *100*, 6927.
(25) Pauley, M. A.; Guan, H.-W.; Wang, C. H.; Jen, A. K.-Y. *J. Chem. Phys*. **1996**, *104*, 7821.
(26) Lindsay, R. J. In *Comprehensive Organic Chemistry*; Barton, D., Ollis, W. D., Eds.; Pergamon Press: Oxford, U.K., 1979; Vol. 2, p 168.
(27) Ford, P.; Rudd, De F. P.; Gaunder, R.; Taube, H. *J. Am. Chem. Soc*. **1968**, *90*, 1187.
(28) Johnson, C. R.; Shepherd, R. E. *Inorg. Chem*. **1983**, *22*, 2439.

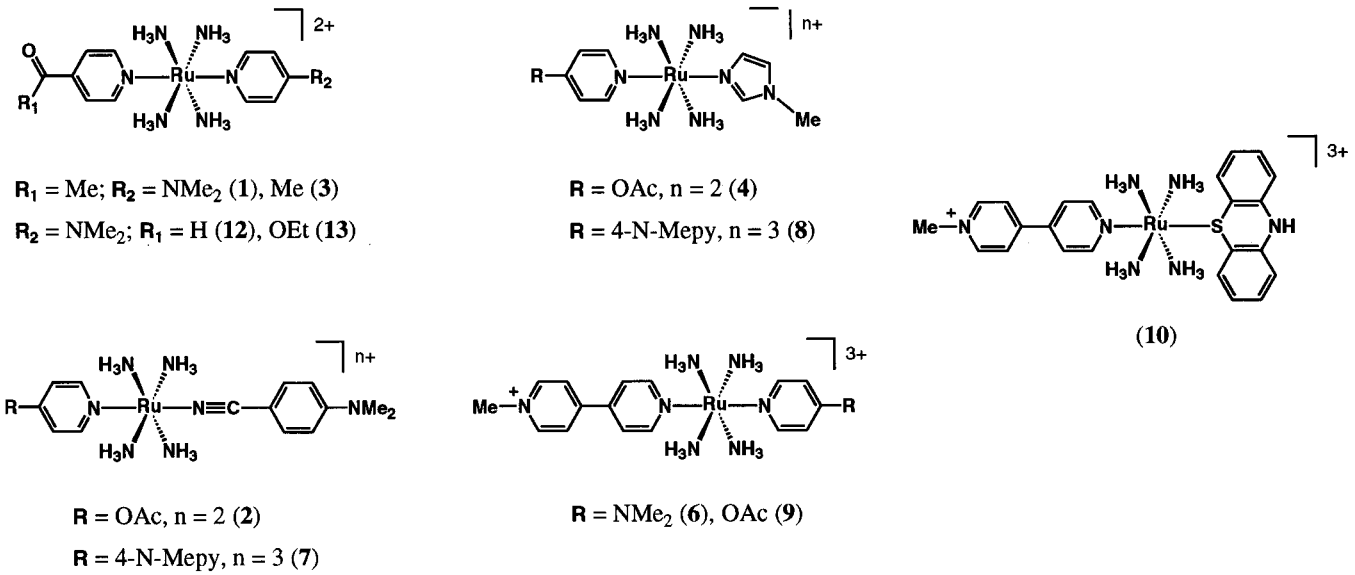

Figure 1. Structures of the complex cations in the salts **1**−**4**, **6**−**10**, **12**, and **13**.

Table 1. UV−Visible and Electrochemical Data Obtained in Acetonitrile

	$E_{1/2}$, V vs SCE (ΔE_p, mV)[a]			
complex salt (no.)	Ru(III/II)	ligand waves	λ_{max} (ϵ), nm (M^{-1} cm^{-1})[b]	assignment
trans-$[Ru(NH_3)_4(4\text{-acpy})(dmap)](PF_6)_2$ (**1**)	0.46 (70)	−1.41 (70)[c]	258 (10 400)	$\pi \rightarrow \pi^*$
			326 (6300)	$d\pi \rightarrow \pi^*$(dmap)
			520 (13 800)	$d\pi \rightarrow \pi^*$(4-acpy)
trans-$[Ru(NH_3)_4(4\text{-acpy})(dmabn)](PF_6)_2$ (**2**)	0.69 (70)	1.33 (70)	228 (20 700)	$\pi \rightarrow \pi^*$
		−1.36 (70)[c]	294 (15 600)	$\pi \rightarrow \pi^*$
			330 (21 800)	$d\pi \rightarrow \pi^*$(dmabn)
			472 (16 400)	$d\pi \rightarrow \pi^*$(4-acpy)
trans-$[Ru(NH_3)_4(4\text{-acpy})(4\text{-pic})](PF_6)_2$ (**3**)	0.61 (80)	−1.35 (80)[c]	248 (5200)	$\pi \rightarrow \pi^*$
			268 (3700)	$\pi \rightarrow \pi^*$
			360 (3400)	$d\pi \rightarrow \pi^*$(4-pic)
			496 (15 300)	$d\pi \rightarrow \pi^*$(4-acpy)
trans-$[Ru(NH_3)_4(4\text{-acpy})(1\text{-MeIm})](PF_6)_2$ (**4**)	0.47 (70)	−1.40 (80)[c]	270 (5800)	$\pi \rightarrow \pi^*$
			364 (800)	d → d
			510 (13 900)	$d\pi \rightarrow \pi^*$(4-acpy)
trans-$[Ru(NH_3)_4(MeQ^+)(dmap)](PF_6)_3$ (**6**)	0.46 (70)	−0.87 (65)	266 (22 700)	$\pi \rightarrow \pi^*$
		−1.46 (70)	332 (6500)	$d\pi \rightarrow \pi^*$(dmap)
			614 (17 200)	$d\pi \rightarrow \pi^*(MeQ^+)$
trans-$[Ru(NH_3)_4(MeQ^+)(dmabn)](PF_6)_3$ (**7**)	0.70 (65)	−0.85 (75)	256 (20 500)	$\pi \rightarrow \pi^*$
		−1.43 (70)	276 (20 200)	$\pi \rightarrow \pi^*$
		1.32 (60)	288 (20 900)	$\pi \rightarrow \pi^*$
			332 (23 900)	$d\pi \rightarrow \pi^*$(dmabn)
			540 (17 700)	$d\pi \rightarrow \pi^*(MeQ^+)$
trans-$[Ru(NH_3)_4(MeQ^+)(1\text{-MeIm})](PF_6)_3$ (**8**)	0.47 (75)	−0.88 (70)	268 (18 100)	$\pi \rightarrow \pi^*$
		−1.48 (65)	330 (1600)	d → d
			602 (16 200)	$d\pi \rightarrow \pi^*(MeQ^+)$
trans-$[Ru(NH_3)_4(MeQ^+)(4\text{-acpy})](PF_6)_3$ (**9**)	0.70 (65)	−0.82 (60)	266 (19 400)	$\pi \rightarrow \pi^*$
		−1.34 (65)	350 (1300)	d → d
			450sh (4300)	$d\pi \rightarrow \pi^*$(4-acpy)
			562 (22 200)	$d\pi \rightarrow \pi^*(MeQ^+)$
trans-$[Ru(NH_3)_4(MeQ^+)(PTZ)](PF_6)_3$ (**10**)	0.90[d]	−0.80 (80)	246 (22 400)	$\pi \rightarrow \pi^*$
		−1.32 (100)	256 (22 400)	$\pi \rightarrow \pi^*$
			498 (8400)	$d\pi \rightarrow \pi^*(MeQ^+)$
trans-$[Ru(NH_3)_4(dmap)(pyca)](PF_6)_2$ (**12**)	0.50 (65)	−1.24[e]	256 (11 900)	$\pi \rightarrow \pi^*$
			322 (7300)	$d\pi \rightarrow \pi^*$(dmap)
			544 (16 600)	$d\pi \rightarrow \pi^*$(pyca)
trans-$[Ru(NH_3)_4(dmap)(isne)](PF_6)_2$ (**13**)	0.47 (65)	−1.63[e]	260 (11 100)	$\pi \rightarrow \pi^*$
			326 (6500)	$d\pi \rightarrow \pi^*$(dmap)
			500 (17 000)	$d\pi \rightarrow \pi^*$(isne)

[a] Measured in solutions *ca.* 10^{-3} M in analyte and 0.1 M in $[N(C_4H_9\text{-}n)_4]PF_6$ at a Pt bead working electrode with a scan rate of 200 mV s^{-1}. Ferrocene internal reference $E_{1/2} = 0.41$ V, $\Delta E_p = 60$ mV. [b] Solutions $(1-4) \times 10^{-5}$ M. [c] Irreversible reduction process as evidenced by $i_{pc} > i_{pa}$. [d] E_{pa} for an irreversible oxidation process. [e] E_{pc} for an irreversible reduction process.

creases in the order L^D = dmap < 1-MeIm < 4-pic < dmabn. This reflects the increasing stability of the Ru donor orbitals as the basicity of L^D decreases. Similarly, for the salts *trans*-$[Ru(NH_3)_4(MeQ^+)(L^D)](PF_6)_3$ (**6**−**10**), the MLCT-1 energy increases in the order L^D = dmap < 1-MeIm < 4-acpy < dmabn < PTZ. In addition to the MLCT bands, all of the complexes show intense, high-energy bands below 300 nm due to intraligand $\pi \rightarrow \pi^*$ excitations.

Solvatochromism is a phenomenon characteristic of MLCT bands[18,29] and is also often indicative of substantial molecular

Table 2. Solvent Parameters and Solvatochromism Data for Salts **6**−**10**

solvent	ϵ_r[a]	DN,[b] kcal mol^{-1}	λ_{max}[MLCT-1], nm (E_{MLCT}, 10^3 cm^{-1}) **6**	**7**	**8**	**9**	**10**
hexamethylphosphoramide, HMPA	31.3	38.8	706 (14.16)	606 (16.50)	686 (14.58)	660 (15.15)	570 (17.54)
dimethyl sulfoxide, DMSO	47.2	29.8	686 (14.58)	592 (16.89)	664 (15.06)	628 (15.92)	546 (18.32)
dimethylformamide, DMF	38.3	26.6	674 (14.84)	582 (17.18)	658 (15.20)	618 (16.18)	542 (18.45)
trimethyl phosphate, TMP	20.6	23.0	668 (14.97)	574 (17.42)	654 (15.29)	614 (16.29)	530 (18.87)
acetone, AC	21.0	17.0	626 (15.97)	548 (18.25)	618 (16.18)	576 (17.36)	508 (19.69)
acetonitrile, AN	36.6	14.1	614 (16.29)	540 (18.52)	602 (16.61)	562 (17.79)	498 (20.08)
nitromethane, NM	37.3	2.7	604 (16.56)	528 (18.94)	590 (16.95)	554 (18.05)	488 (20.49)
$\Delta\lambda$, nm[c]			102	78	96	106	82
ΔE, cm^{-1} [d]			2392	2438	2372	2899	2948

[a] ϵ_r = relative permittivity (dielectric constant) of solvent at 20 °C. Source: *CRC Handbook of Chemistry and Physics*, 75th ed.; Lide, D. R., Ed.; CRC Press: Boca Raton, FL, 1994. [b] Gutmann donor number.[31] [c] Difference between maximum and minimum wavelengths. [d] Difference between maximum and minimum energies.

Table 3. Crystallographic Data and Refinement Details for *trans*-$[Ru(NH_3)_4(MeQ^+)(PTZ)](PF_6)_3 \cdot Me_2CO$ (**10**·Me_2CO)

formula	$C_{26}H_{38}F_{18}N_7OP_3RuS$
M_r	1032.7
crystal system	hexagonal
space group	$P6_3$
a, Å	17.853(4)
b, Å	17.853(4)
c, Å	21.514(6)
V, Å^3	5939(3)
Z	6
D_c, g cm^{-3}	1.73
T, °C	−100(2)
λ, Å	0.710 73 (Mo Kα)
F(000)	3108
μ, cm^{-1}	6.89
scan type	ω
2θ limit, deg	50.0
h, k, l ranges	−21/15, −21/20, −25/25
no. of reflns collected	28341
no. of unique reflns (R_{int})	7018 (0.0266)
no. of obsd reflns	7017 [$I > 2\sigma(I)$]
final R indices[a]	$R_1 = 0.0321$, w$R_2 = 0.0845$
R indices (all data)[a]	$R_1 = 0.0333$, w$R_2 = 0.0864$
goodness of fit, S	1.057
no. of parameters	526
peak and hole, e Å^{-3}	0.753, −0.304

[a] $R_1 = \sum(||F_o| - |F_c||)/\sum|F_o|$; w$R_2 = [\sum w(F_o^2 - F_c^2)^2/\sum w(F_o^2)^2]^{1/2}$; $S = [\sum w(F_o^2 - F_c^2)^2/(M - N)]^{1/2}$, where M = number of reflections and N = number of parameters.

β values.[30] Previous studies on the solvatochromism in dipolar aprotic solvents of *trans*-$\{Ru(NH_3)_4\}^{2+}$ complexes show that the MLCT-1 band energies do not correlate with solvent dielectric constants but rather with the solvent (Gutmann) donor numbers.[18] This was rationalized by invoking hydrogen-bonding between solvent molecules and ammine ligands, which increases the electron density at the Ru center, stabilizing Ru(III), hence shifting the MLCT-1 transition to lower energy. Further support for this hypothesis was obtained by good correlations between MLCT-1 energies and other solvent scales which are based on the hydrogen-bond-accepting ability of the solvent.[18] A much lesser degree of solvatochromism was observed for the MLCT-2 absorptions.

A limited solvatochromism study was carried out with the series **6**−**10**, and results are presented in Table 2. As expected, all of the salts show a good correlation between the MLCT-1 energy and the Gutmann donor numbers (DN)[31] (Figure 2; data shown for **7**, **8**, and **10**), with excitation maxima moving to lower energy as solvent donor capacity increases. The similar slopes show that the degree of solvatochromism is roughly equivalent within this series of complexes.

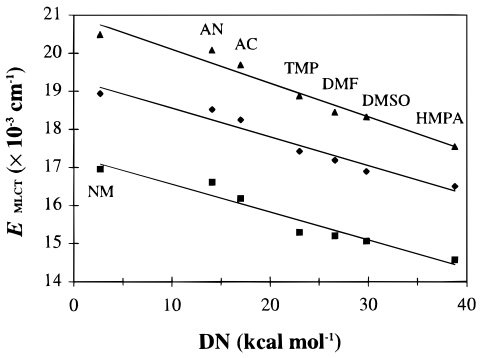

Figure 2. MLCT-1 energies as a function of solvent Gutmann donor number for the salts **7** (♦), **8** (■), and **10** (▲). See Table 2 for definition of solvent abbreviations.

Table 4. Selected Bond Distances (Å) and Angles (deg) for **10**·Me_2CO

Ru−N(31)	2.095(4)	S−C(12)	1.779(6)
Ru−N(1)	2.163(5)	S−C(22)	1.771(6)
Ru−N(2)	2.141(5)	N(11)−C(11)	1.393(7)
Ru−N(3)	2.135(5)	N(11)−C(21)	1.386(8)
Ru−N(4)	2.130(5)	N(11)−H(11)	0.73(8)
Ru−S	2.3283(13)		
N(31)−Ru−N(1)	89.2(2)	N(2)−Ru−N(3)	92.0(2)
N(31)−Ru−N(2)	89.0(2)	N(2)−Ru−N(4)	179.1(2)
N(31)−Ru−N(3)	89.7(2)	N(2)−Ru−S	93.47(14)
N(31)−Ru−N(4)	90.9(2)	N(3)−Ru−N(4)	87.1(2)
N(31)−Ru−S	177.02(11)	N(3)−Ru−S	88.60(14)
N(1)−Ru−N(2)	89.4(2)	N(4)−Ru−S	86.56(13)
N(1)−Ru−N(3)	178.1(2)	C(12)−S−Ru	110.1(2)
N(1)−Ru−N(4)	91.5(2)	C(22)−S−Ru	112.0(2)
N(1)−Ru−S	92.50(13)	C(22)−S−C(12)	98.6(2)

Electrochemical Studies. All of the complex salts, except for **5** and **11**, were studied by cyclic voltammetry in acetonitrile, and results are presented in Table 1.

All except **10** exhibit reversible or quasi-reversible (ΔE_p > 70 mV) Ru(III/II) oxidation waves at potentials which are in accord with expectation.[32] Within the series *trans*-$[Ru(NH_3)_4(4\text{-acpy})(L^D)](PF_6)_2$ (**1**−**4**), $E_{1/2}$ becomes more positive in the order L^D = dmap ≈ 1-MeIm < 4-pic < dmabn, as the decreasing basicity of L^D stabilizes the Ru-based HOMO. Similarly, for the salts *trans*-$[Ru(NH_3)_4(MeQ^+)(L^D)](PF_6)_3$ (**6**−**9**), $E_{1/2}$ becomes more positive in the order L^D = dmap ≈ 1-MeIm < 4-acpy ≈ dmabn. As expected, these trends follow the order of increasing MLCT-1 energies. The irreversible oxidation behavior of **10** arises from complications due to the PTZ ligand, which undergoes oxidation to the $PTZ^{\bullet+}$ cation radical. Similar redox behavior has been reported for *cis*- and *trans*-$[Ru(bpy)_2(PTZ)_2](PF_6)_2$.[33]

(29) Creutz, C.; Chou, M. H. *Inorg. Chem.* **1987**, *26*, 2995.
(30) Paley, M. S.; Harris, J. M. *J. Org. Chem.* **1991**, *56*, 568.
(31) Gutmann, V. *The Donor-Acceptor Approach to Molecular Interactions*; Plenum: New York, 1978.
(32) Lever, A. B. P. *Inorg. Chem.* **1990**, *29*, 1271.

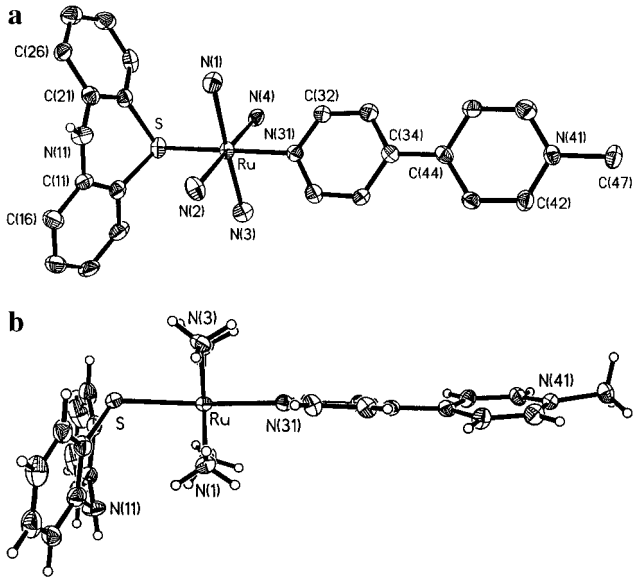

Figure 3. (a) Structural representation of the cation in **10**·Me_2CO, *trans*-$[Ru(NH_3)_4(MeQ^+)(PTZ)]^{3+}$, with unrefined hydrogen atoms omitted. The thermal ellipsoids correspond to 50% probability. (b) Alternative view of the cation *trans*-$[Ru(NH_3)_4(MeQ^+)(PTZ)]^{3+}$, showing the coordination mode of the PTZ ligand and the pseudoplanarity of the MeQ^+ ligand.

The salt $[MeQ^+]PF_6$ exhibits two reversible one-electron reduction waves at −0.92 and −1.61 V vs SCE, assigned to the $MeQ^{+/0}$ and $MeQ^{0/-}$ redox couples, respectively.[34] Each of the complexes in **6**−**10** shows two corresponding reversible or quasi-reversible reduction waves in the regions −0.80 to −0.87 V and −1.33 to −1.46 V vs SCE. Coordination to a *trans*-$\{Ru(NH_3)_4(L^D)\}^{2+}$ center hence produces shifts of +50−120 mV in the $MeQ^{+/0}$ couple and of +150−280 mV in the $MeQ^{0/-}$ couple due to stabilization of the MeQ^+-based LUMO. These $E_{1/2}$ values become more negative in the order L^D = PTZ < 4-acpy < dmabn < 1-MeIm ≈ dmap, reflecting the increasing basicity of L^D. In addition, irreversible reduction waves are observed for **1**−**4**, **12**, and **13** which are assigned to reductions of the 4-acpy, pyca, and isne ligands.

The dmabn ligand in **2** and **7** gives a single reversible or quasi-reversible oxidation wave which is shifted by *ca*. +200 mV from the value of 1.16 V vs SCE reported for the free ligand.[35] This anodic shift is due to transmission of the electron-withdrawing influence of the Ru(III) center via the nitrile group.

Structural Determination. A single-crystal X-ray structure was obtained for **10**·Me_2CO. Two alternative representations of the cation are shown in Figure 3. The acetone of crystallization is strongly bound due to H-bonding with two ammine ligands and with one PF_6^- anion.

The complex in **10**·Me_2CO has the expected *trans* geometry (Figure 3a), with the plane of the coordinated pyridyl ring bisecting the $N(NH_3)-Ru-N(NH_3)$ angles to give a N(1)−Ru(1)−N(31)−C(32) torsion angle of −42.4° (Figure 3b). The MeQ^+ ligand adopts an almost planar conformation with only a small twist between the two pyridyl rings, giving a C(35)−C(34)−C−(44)−C(43) torsion angle of 9.6°. This implies that electronic delocalization between the two pyridyl rings in the solid state largely overcomes the steric repulsion between the 3,3′- and 5,5′-hydrogen atoms. However, no evidence for a significant quinoidal contribution is observed in the bond lengths. The inter-ring bond C(34)−C(44) of 1.485(6) Å is significantly longer than the intra-ring bonds (*e.g.*, C(32)−C(33) is 1.391(8) Å), and the Ru−N(31) bond distance of 2.095(4) Å is not unusually short.[36] It can be reasonably assumed that free rotation about the inter-ring C−C bond occurs in solutions of **10** and of the other MeQ^+ complexes in **6**−**9**,[37] but the low-energy $d\pi(Ru^{II}) \rightarrow \pi^*(MeQ^+)$ MLCT absorption shows that inter-ring electronic coupling is nevertheless extensive.[37]

A large number of Ru(II)−MeQ^+ complexes have been synthesized, but since **10**·Me_2CO is the first to be structurally characterized, no direct comparisons can be made. The mixed-valence triruthenium cluster salt $[Ru_3(\mu_3\text{-}O)(\mu\text{-}CH_3CO_2)_6(MeQ^+)_2(CO)](ClO_4)_2$·2DMF contains MeQ^+ coordinated to the Ru(III) centers, but no torsion angles were reported.[34] In *fac*-$[Re(CO)_3(bpy)(MeQ^+)](PF_6)_2$[37] and in *fac*-$[Re(CO)_3(bpm)(MeQ^+)](PF_6)_2$·MeCN (bpm = 2,2′-bipyrimidine),[38] the MeQ^+ ligands adopt twisted conformations with dihedral angles between the pyridyl rings of 47 and 38°, respectively.

The "side-on" coordination mode of the sulfur-bound PTZ ligand in **10**·Me_2CO (Figure 3b), with a Ru−S−C bond angle of 110.1(2)°, is similar to that observed in *cis*-$[Ru(bpy)_2(PTZ)_2](PF_6)_2$·$0.5H_2O$ and in *trans*-$[Ru(bpy)_2(PTZ)_2](PF_6)_2$·$H_2O$.[33] In the latter complexes, the Ru−S bond lengths of 2.381(16) and 2.347(2) Å, respectively, are a little longer than that in **10**·Me_2CO. Other dimensions of the PTZ ligand are very similar in all three complexes.

The solid-state requirement for quadratic NLO effects[1] is met by the crystallization of **10**·Me_2CO in the noncentrosymmetric hexagonal space group $P6_3$. The complex cations adopt a spiral packing arrangement (Figure 4), producing a strong projected component along the polar *z* axis. However, since the crystal twinning will produce a net dipole cancellation at the macroscopic level, no bulk SHG is anticipated.

Nonlinear Optical Studies. The first hyperpolarizabilities β of most of the new complexes were measured in acetonitrile using the HRS technique[16,17,22] with a 1064 nm Nd:YAG laser fundamental. Results are presented in Table 5, together with the MLCT-1 band maxima and energies.

The β values obtained are very large, and similar to those previously reported for other Ru complexes.[7−9] The clearest trend is that the β values for **6**−**8**, which contain MeQ^+ as L^A, are approximately twice those of their analogues containing 4-acpy, pyca, or isne. This can be ascribed to two interconnected factors which are known to enhance β in organic molecules.[1] First, the *N*-methylpyridinium-4-yl group is a more powerful electron acceptor than the 4-acetyl, formyl, and ethyl ester groups, a fact reflected in the lower MLCT-1 energies for **6**−**8** compared to **1**, **2**, **4**, **12**, and **13**. A direct comparison is provided by the energy separation of *ca*. 4430 cm^{-1} between the two visible MLCT bands in **9** (*vide supra*). Also, **6**−**8** feature an increased conjugation length, containing (potentially) three aromatic rings rather than two. The crystallographic study of **10**·Me_2CO (*vide supra*) shows that the electronic coupling within the MeQ^+ ligand is strong enough to induce an almost planar conformation, and it is likely that L^D is coplanar.[13]

It is established for dipolar organics that a linear correlation exists between β and the energy of the intramolecular charge-transfer (ICT) absorption which is the primary contributor to β. The latter increases as the ICT band maximum shifts to lower energy, either as a result of chemical modifications[39] or because

(33) Kroener, R.; Heeg, M. J.; Deutsch, E. *Inorg. Chem.* **1988**, *27*, 558.
(34) Abe, M.; Sasaki, Y.; Yamada, Y.; Tsukahara, K.; Yano, S.; Yamaguchi, T.; Tominaga, M.; Taniguchi, I.; Ito, T. *Inorg. Chem.* **1996**, *35*, 6724.
(35) Perkins, T. A.; Pourreau, D. B.; Netzel, T. L.; Schanze, K. S. *J. Phys. Chem.* **1989**, *93*, 4511.
(36) Wishart, J. F.; Bino, A.; Taube, H. *Inorg. Chem.* **1986**, *25*, 3318.
(37) Chen, P.; Curry, M.; Meyer, T. J. *Inorg. Chem.* **1989**, *28*, 2271.
(38) Winslow, L. N.; Rillema, D. P.; Welch, J. H.; Singh, P. *Inorg. Chem.* **1989**, *28*, 1596.

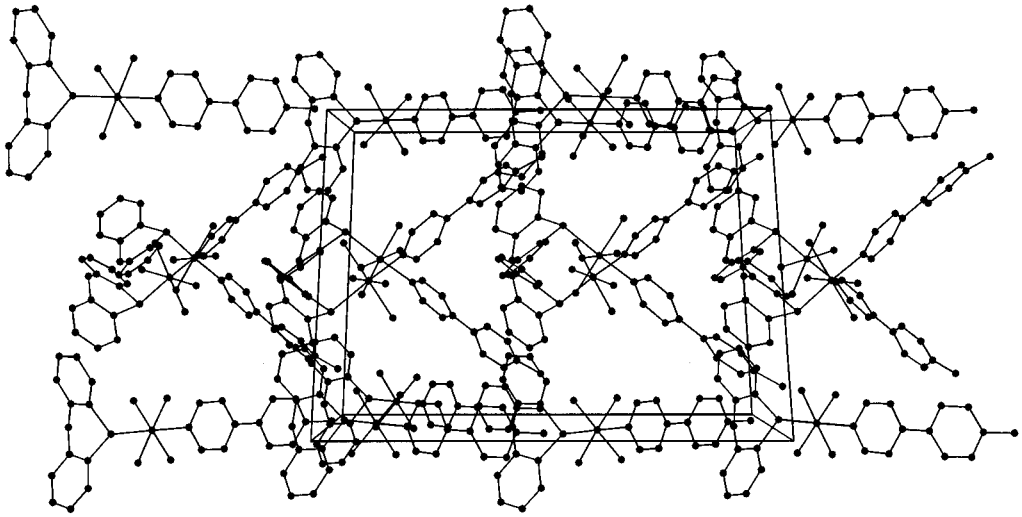

Figure 4. Crystal-packing diagram for **10**·Me_2CO, showing the alignment of the dipolar cations along the *z* axis.

Table 5. Linear and Nonlinear Optical Data Obtained in Acetonitrile

complex salt (no.)	λ_{max}[MLCT-1], nm	E_{MLCT}, 10^3 cm^{-1}	β_{1064},[a] 10^{-30} esu	β_0,[a] 10^{-30} esu
trans-[$Ru(NH_3)_4$(4-acpy)(dmap)]$(PF_6)_2$ (**1**)	520	19.23	284	10
trans-[$Ru(NH_3)_4$(4-acpy)(dmabn)]$(PF_6)_2$ (**2**)	472	21.19	310	53
trans-[$Ru(NH_3)_4$(4-acpy)(1-MeIm)]$(PF_6)_2$ (**4**)	510	19.61	232	14
trans-[$Ru(NH_3)_4$(MeQ^+)(dmap)]$(PF_6)_3$ (**6**)	614	16.29	587	130
trans-[$Ru(NH_3)_4$(MeQ^+)(dmabn)]$(PF_6)_3$ (**7**)	540	18.52	621	14
trans-[$Ru(NH_3)_4$(MeQ^+)(1-MeIm)]$(PF_6)_3$ (**8**)	602	16.61	523	100
trans-[$Ru(NH_3)_4$(MeQ^+)(4-acpy)]$(PF_6)_3$ (**9**)	562	17.79	550	46
trans-[$Ru(NH_3)_4$(MeQ^+)(PTZ)]$(PF_6)_3$ (**10**)	498	20.08	419	40
trans-[$Ru(NH_3)_4$(dmap)(pyca)]$(PF_6)_2$ (**12**)	544	18.38	362	12
trans-[$Ru(NH_3)_4$(dmap)(isne)]$(PF_6)_2$ (**13**)	500	20.00	302	27

[a] β_{1064} is the uncorrected first hyperpolarizability measured using a 1064 nm Nd:YAG laser fundamental; β_0 is the static hyperpolarizability estimated by using the two-level model (eq 1). The quoted cgs units (esu) can be converted into SI units (C^3 m^3 J^{-2}) by dividing by a factor of 2.693×10^{20}.

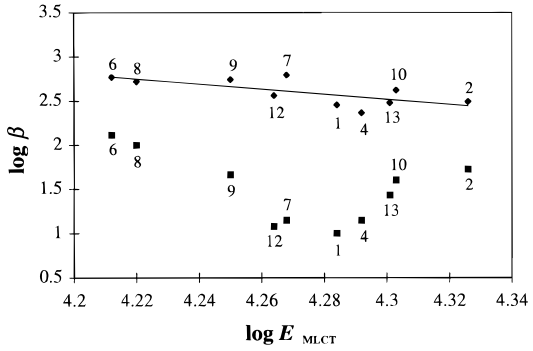

Figure 5. Log−log plot of the first hyperpolarizability against the MLCT-1 energy for the salts **1**, **2**, **4**, **6**−**10**, **12**, and **13** (♦ = log β; ■ = log β_0).

of changes in the solvent medium.[23] Due to a lack of empirical data, a parallel relationship has not been demonstrated previously for transition metal coordination complexes. The marked solvatochromism of the MLCT-1 bands in these *trans*-{$Ru(NH_3)_4$}$^{2+}$ complexes (*vide supra*) confirms that these excitations are the primary contributors to β. It is hence not surprising that a good linear correlation and a negative slope are found in a plot of log β vs log E_{MLCT}, where E_{MLCT} is the MLCT-1 energy (Figure 5).

Because these complexes absorb strongly in the region of the second harmonic at 532 nm, the high magnitude of their β values is attributed in part to resonance enhancement. This phenomenon can be explained by means of the two-level model,[40] which is valid in cases where β is dominated by a single ICT transition. According to this approximation, the relationship between the first hyperpolarizability and the optical ICT excitation is described by

$$\beta(-2\omega;\omega,\omega) = \frac{3\Delta\mu M^2}{(h\omega_{CT})^2}\frac{\omega_{CT}^2}{[1-(2\omega)^2(\omega_{CT}^2)^{-1}][(\omega_{CT})^2-\omega^2]} = \beta_0\frac{\omega_{CT}^2}{[1-(2\omega)^2(\omega_{CT}^2)^{-1}][(\omega_{CT})^2-\omega^2]} \quad (1)$$

where $h\omega_{CT}$ is the energy of the ICT excitation, $\Delta\mu$ is the change in dipole moment between the ground state and one excited state, M is the electronic transition moment, ω is the fundamental laser frequency (in cm^{-1}), and β_0 is the static (corrected) hyperpolarizability. Values of β_0, which is an estimate of the intrinsic molecular hyperpolarizability, calculated by using eq 1 with ω_{CT} being E_{MLCT}, are listed in Table 5.

The corrected hyperpolarizabilities highlight some further contrasts between the complexes. For the 4-acpy salts **1**, **2**, and **4**, the uncorrected β values are not significantly different, but the dmabn salt **2** has by far the largest β_0. This is partly because a neglect of damping in the two-level model causes underestimation of β_0 when the absorption maximum is close

(39) See, for example: (a) Cheng, L.-T.; Tam, W.; Meredith, G. R.; Rikken, G.; Meijer, E. *Proc. SPIE-Int. Soc. Opt. Eng.* **1989**, *1147*, 61. (b) Stiegman, A. E.; Graham, E.; Perry, K. J.; Khundkar, L. R.; Cheng, L.-T.; Perry, J. W. *J. Am. Chem. Soc.* **1991**, *113*, 7658.

(40) (a) Oudar, J. L.; Chemla, D. S. *J. Chem. Phys.* **1977**, *66*, 2664. (b) Oudar, J. L. *J. Chem. Phys.* **1977**, *67*, 446. (c) Zyss, J.; Oudar, J. L. *Phys. Rev. A* **1982**, *26*, 2016.

to the second-harmonic frequency (*e.g.*, for **1** and **4**). However, **2** clearly has the largest hyperpolarizability of **1**, **2**, or **4** since it has the largest resonance-enhanced β, although its absorption maximum is further from 532 nm than are those of **1** and **4**. The underestimation of β_0 for **1** and **4** merely exaggerates this difference.

Of the MeQ^+ salts, **6** and **8** have the largest β_0 values by a considerable margin. This is because the high basicity of the dmap or 1-MeIm ligands stabilizes Ru(III) and hence causes the MLCT-1 bands to occur at particularly low energy. The corrected hyperpolarizabilities for **6** and **8** are an order of magnitude larger than those of their 4-acpy analogues, but this is partly due to the underestimation of the values for **1** and **4**. Despite having the largest β, **7** has a β_0 which is among the lowest of the complexes studied. This is because the close proximity of the MLCT-1 absorption to 532 nm leads to a gross underestimation of β_0. Due to the neglect of damping effect, a plot of log β_0 vs log E_{MLCT} (Figure 5) shows only a partial correlation. Only the points for **2**, **6**, **8**, **10**, and **13** fall on a reasonable straight line, the extent of underestimation of β_0 being greatest for **1**, **4**, **7**, and **12**.

Conclusions

The complexes *trans*-$[Ru(NH_3)_4(L^A)(L^D)]^{n+}$ ($n = 2, 3$) where L^A and L^D are acceptor/donor functionalized ligands exhibit very large first hyperpolarizabilities β at 1064 nm due in part to resonance enhancement. β correlates well with the energy of the lowest energy MLCT absorption, confirming that this excitation is the primary contributor to the hyperpolarizability. A similar correlation for β_0 is only evident for the complexes in which the MLCT absorption is sufficiently far from 532 nm. Current synthetic work is aimed at widening the range of ligand combinations to allow the maximization of β and the establishment of further structure−property correlations. In cases where the Ru(III/II) reduction potential is readily accessible, the effects or metal-based redox changes on the NLO properties are also to be investigated.

Acknowledgment. S.H. is a Research Assistant of the Belgian National Fund for Scientific Research. This work was supported by research grants from the The Royal Society, from the Belgian National Fund for Scientific Research (G.2103.93 and 9.0011.92), from the Belgian Government (IUAP-16), and from the University of Leuven (GOA/1/95). Thanks are expressed to Johnson Matthey plc for a generous loan of ruthenium trichloride.

Supporting Information Available: Tables of final atomic fractional coordinates, thermal parameters, and nonessential bond lengths and angles (11 pages). Ordering information is given on any current masthead page.

IC961465M